Roughness Induced Boundary Slip in Microchannel Flows

Christian Kunert and Jens Harting

Institute for Computational Physics, University of Stuttgart, Pfaffenwaldring 27, D-70569 Stuttgart, Germany

(Received 24 April 2007; published 23 October 2007)

Surface roughness becomes relevant if typical length scales of the system are comparable to the variations as it is the case in microfluidic setups. Here, an apparent slip is often detected which can have its origin in the misleading assumption of perfectly smooth boundaries. We investigate the problem by means of lattice Boltzmann simulations and introduce an ''effective no-slip plane'' at an intermediate position between peaks and valleys of the surface. Our simulations agree with analytical results for sinusoidal boundaries, but can be extended to arbitrary geometries and experimentally obtained data. We find that the apparent slip is independent of the detailed boundary shape, but only given by the distribution of surface heights. Further, we show that slip diverges as the amplitude of the roughness increases which highlights the importance of a proper treatment of surface variations in very confined geometries.

DOI: 10.1103/PhysRevLett.99.176001 PACS numbers: 83.50.Rp, 47.61.−k, 68.08.−p

In microfluidic systems the surface to volume ratio is large causing boundary effects to be significantly more important than in macroscopic devices. Since even on atomic or molecular scales a perfectly smooth surface is an idealized model, the shape of the boundary is an important property. Additionally, it is of technological interest to design surfaces with well defined structures and properties [1,2]. A commonly investigated surface property is the apparent slip originating, for example, from the surface wettability, electrostatic interactions, impurities, or surface structuring [3]. Navier characterized hydrodynamic slip by postulating that the fluid velocity $v(x)$ at the boundary ($x = 0$) is proportional to the shear rate $\frac{\partial v}{\partial x}$ and the slip length β [4]. For macroscopic systems the simple no-slip condition ($\beta = 0$) is a valid assumption. However, if the height of surface variations is not small compared to typical length scales of the system, the position of the boundary is not clearly defined and experiments might detect slip due inaccurately determined wall positions. The influence of roughness on the slip length β has been investigated by numerous authors. Roughness leads to higher drag forces and thus to no-slip on macroscopic scales, as shown by Richardson [5] and Jansons [6]. This was experimentally demonstrated by McHale and Newton [7]. Jabbarzadeh *et al.* performed molecular dynamics (MD) simulations of Couette flow between sinusoidal walls and found that slip appears for roughness amplitudes smaller than the molecular length scale [8]. Also, it can cause pockets to be filled with vapor or gas nano bubbles leading to apparent slip [2,9]. Recently, Sbragaglia *et al.* applied the LB method to simulate fluids in the vicinity of microstructured hydrophobic surfaces [10] and Varnik *et al.* [11] have shown that even in small geometries rough channel surfaces can cause flow to become turbulent. A common setup to measure slip is to utilize a modified atomic force microscope (AFM) to oscillate a colloidal sphere in the vicinity of a boundary [12–14]. Vinogradova and Yakubov demonstrated that assuming a wrong position of the surface during measurements can lead to substantial errors in the determined slip lengths [14]. They showed that measurements can be interpreted by assuming a modified sphere radius instead of Navier's slip condition, so that the position of a no-slip wall would be between peaks and valleys of the rough surface. In this Letter we follow this idea. We answer the question at which position the ''effective boundary'' has to be placed and study the influence of a wrongly determined wall position numerically.

Panzer *et al.* gave an analytical equation for β for small cosine-shaped surface variations [15]. It is applicable to infinite planes separated by a distance $2d$ being much larger than the highest peaks $h_{\max}$. Surface variations are determined by peaks of height $h_{\max}$, valleys at $h_{\min}$ and given by $h(z) = h_{\max}/2 + h_{\max}/2\cos(qz)$. Here, q is the wave number and the corresponding slip length is found to be

$$\beta = \frac{-h_{\max}}{2}\left(1 + k\frac{1 - \frac{1}{4}k^2 + \frac{19}{64}k^4 + \mathcal{O}(k^6)}{1 + k^2(1 - \frac{1}{2}k^2) + \mathcal{O}(k^6)}\right). \quad (1)$$

Higher-order terms cannot easily be calculated analytically and are neglected. Thus, Eq. (1) is valid only for $k = qh_{\max}/2 \ll 1$. However, for realistic surfaces, k can become substantially larger than 1 causing the theoretical approach to fail. Here, only numerical simulations can be applied to describe arbitrary boundaries.

We use a 3D LB model as presented in [16–18] to simulate pressure driven flow between infinite rough walls. Previously, we applied the method to study flows of simple fluids and complex mixtures containing surfactant in hydrophobic microchannels [18,19]. Here, we only shortly describe our method and refer to the literature for details. The lattice Boltzmann equation, $\eta_i(\mathbf{x} + \mathbf{c}_i, t + 1) - \eta_i(\mathbf{x}, t) = \Omega_i$, with $i = 0, 1, \ldots, b$, describes the time evolution of the single-particle distribution $\eta_i(\mathbf{x}, t)$, indicating the amount of quasi particles with velocity $\mathbf{c}_i$, at site $\mathbf{x}$ on a 3D lattice of coordination number $b = 19$, at time-step t.

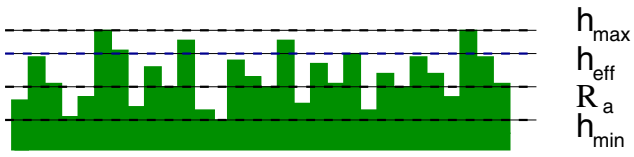

FIG. 1 (color online). (Color online) The effective boundary at h_{eff} is found between deepest valleys (h_{min}) and highest peaks (h_{max}).

We choose the Bhatnagar-Gross-Krook collision operator $\Omega_i = -\tau^{-1}[\eta_i(\mathbf{x}, t) - \eta_i^{\text{eq}}(\mathbf{u}(\mathbf{x}, t), \eta(\mathbf{x}, t))]$, with mean collision time $\tau = 1$ and equilibrium distribution η_i^{eq} [16,18]. Simulation lattices are 256 lattice units long in flow direction and the planes are separated by 62 sites. Periodic boundary conditions are imposed in the remaining direction allowing us to keep the resolution as low as 16 lattice units. A pressure gradient is obtained as described in [18] and midgrid bounce-back boundaries are applied at the surfaces. An effective boundary position can be found by fitting the parabolic flow profile

$$v_z(x) = \frac{1}{2\mu}\frac{\partial P}{\partial z}[d^2 - x^2 - 2d\beta] \tag{2}$$

via the distance $2d = 2d_{\text{eff}}$. β is set to 0 here and viscosity μ as well as pressure gradient $\frac{\partial P}{\partial z}$ are given by the simulation. To obtain an average value for d_{eff}, a sufficient number of individual profiles at different positions z are taken into account. Alternatively, the mass flow $\int v(x)\rho dx$ can be computed to obtain $2d_{\text{eff}}$. Both methods are equivalent and produce identical results. d_{eff} gives the position of the effective boundary and the effective height h_{eff} of the rough surface is then defined by $d - d_{\text{eff}}$ (see Fig. 1).

As rough model surfaces we choose a randomly generated roughness and 3 periodic ones for which the average height or average roughness R_a is given by $h_{\text{max}}/2$. While random surfaces are truly uncorrelated, periodic structures correspond to transverse stripes. Cosine-shaped boundaries are given by $h(x) = h_{\text{max}}/2 + h_{\text{max}}/2\cos(qx)$, squares have a height of h_{max} and are separated by h_{max} lattice sites. Triangular structures are $2h_{\text{max}}$ wide and h_{max} high (see Fig. 2). Randomly generated surface structures are created by choosing for every lattice position of the boundary the height $h(x)$ as a random integer between 0 and h_{max}. For determining h_{eff} we average over 5 surfaces generated with different sequences of uniformly distributed random numbers. All walls are geometrically similar; i.e., the effective height h_{eff} scales linearly with h_{max}.

In Fig. 3 the effective height h_{eff} obtained from our simulations is plotted versus R_a for cosine-shaped surfaces with $qh_{\text{max}}/2 = k = 1, \frac{1}{2}, \frac{1}{3}$ (symbols). Error bars would be smaller than the symbols and are therefore not shown. Lines are given by the analytical solution of Eq. (1). For $k < 1$ the simulated data agrees within 2.5% with Panzer's prediction. However, for $k = 1$ a substantial deviation between numerical and analytical solutions can be observed because Eq. (1) is valid for small k only. The inset of Fig. 3 depicts the ratio of β/h_{max} according to the theory of Panzer. In the case of large $k > 1$, the theory is not able to correctly reproduce the increase of β with increasing h_{max} anymore. Instead, β/h_{max} becomes smaller again due to missing higher order contributions in Eq. (1). Our simulations do not suffer from such limitations allowing us to study arbitrarily complex surfaces.

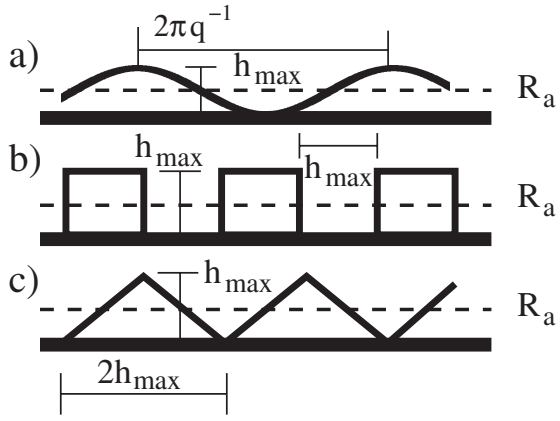

FIG. 2. Periodic surfaces: (a) cosines given by $h(x) = h_{\text{max}}/2 + h_{\text{max}}/2\cos(qx)$. (b) squares with height and separation given by h_{max}. (c) triangles, h_{max} high and $2h_{\text{max}}$ wide.

In Fig. 4(a) h_{eff} is plotted versus R_a for different types of roughness. By performing a linear fit to the data as given by the lines we find for the uniformly distributed roughness that the position of the effective wall is at $c = 1.84$ times the average height of the roughness $R_a = h_{\text{max}}/2$ or at 92% of the maximum height h_{max}. For squares and triangular structures we find constants of proportionality of $c = 1.90$ and $c = 1.69$ indicating that the shape of the surface variations indeed affects the position of the effective

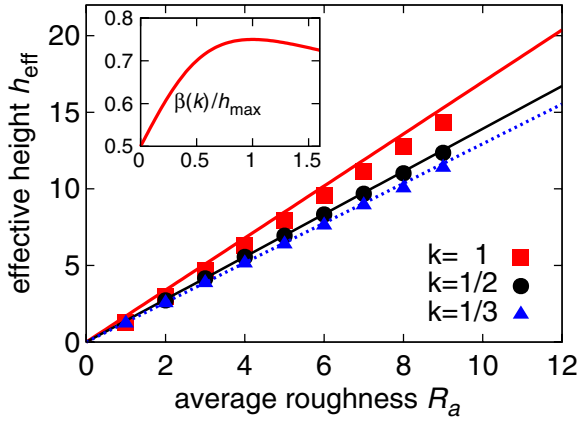

FIG. 3 (color online). (Color online) Effective height h_{eff} over average roughness R_a for a cosine geometry and different variations k. Symbols denote numerical data and lines are given by Eq. (1). The inset shows $\beta(k)/h_{\text{max}}$ according to Eq. (1). For $k > 1$ the slope becomes negative, demonstrating that the theory fails for more complex surface structures.

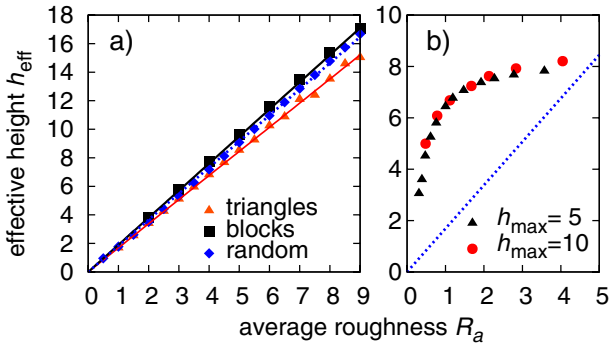

FIG. 4 (color online). (Color online) (a) Effective height h_{eff} versus R_a for triangles, blocks (see Fig. 2), and an equally distributed random roughness. (b) h_{eff} versus R_a for triangles with $h_{\mathrm{max}} = 5$ and 10. The distance between triangles a is varied to obtain the given R_a. Values of $h_{\mathrm{max}} = 5$ are scaled by a factor of 2.

boundary. However, the effect of the shape is small compared to the effect of the height of the variations. All surface structures are geometrically similar causing the linear dependence between h_{eff} and $R_a = h_{\mathrm{max}}/2$ and c being independent of the lattice resolution. When converting our 3D random roughness into a purely 2D structure, the difference in the measured constant of proportionality c is in the range of the error of the fit algorithm. This is a surprising result since in 3D the flow can pass sidewise around a roughness element. The measured h_{eff} is found to be independent of the flow velocity over more than 3 decades and does not depend on pressure either; i.e., h_{eff} is independent of the Reynolds number.

In reality high spikes on a smooth surface may occur, so that the average roughness R_a is much smaller than the maximum height h_{max}. To observe such cases we simulate a triangle geometry with additional void space a between the roughness elements. As maximum height h_{max} we choose 5 and 10 lattice sites. In similarity to Fig. 4(a) we plot the effective surface height h_{eff} over the average roughness R_a in Fig. 4(b). In this case the average roughness is smaller than the half of h_{max}, i.e., $R_a = \frac{h_{\mathrm{max}}^2}{2h_{\mathrm{max}}+a} \leq h_{\mathrm{max}}/2$. The values of $h_{\mathrm{max}} = 5$ are scaled by a factor of 2 to fit them with the values of $h_{\mathrm{max}} = 10$. Because of the geometrical similarity of the surface structure this scaling is possible. For comparison with Fig. 4(a) the linear fit with slope $c = 1.69$ is plotted. In Fig. 4(b) we see that the maximum height has the strongest influence on the effective height h_{eff} and not the distance a. For small R_a created by a large additional distance a, h_{eff} converges to zero corresponding to a flat surface. For small a the data converge to the triangle geometry as given in Fig. 4(a). For a medium $a \approx 2h_{\mathrm{max}}$ the effective wall is still in the range of 75% of the maximum height h_{max}. This is an important result, since it demonstrates that the distance between h_{eff} and h_{min} can be much larger than R_a and that in such cases $h_{\mathrm{eff}} > 6R_a$ can be obtained. On the other hand, for large a this results in $h_{\mathrm{eff}} < 0.7h_{\mathrm{max}}$. Therefore, in the case of large $a \approx 2h_{\mathrm{max}}$, the effective wall h_{eff} cannot be approximated by the maximum height h_{max} nor by the average roughness R_a.

We obtained AFM data of a gold coated glass surface with a maximum peak to valley distance of 64 nm. The sample size is 1 μm^2 represented by 512×512 data points. A lattice constant of the LB simulation can be scaled to 1.9 nm by setting the relaxation time τ to 1.15 and by mapping the speed of sound and the viscosity to the values for water ($c_s = 1.5 \times 10^3$ m/s, $\mu = 1.02 \times 10^{-6}$ m^2/s). h_{eff} can then be measured as in previous paragraphs of this Letter by loading the AFM data onto our simulation lattice. For the simulations presented in this paragraph, the channel width is set to 128 lattice units. The simulated effective height of the gold surface is depicted by the square at $R_a = 21$ nm in Fig. 5. Data points at $R_a = 4$ and 8 are obtained by downscaling the original data set. We find that the distribution of surface heights follows a Gaussian distribution and use this distribution to generate an artificial random surface with identical height distribution. In contrast to the AFM data, our data points are fully uncorrelated, while the gold surface shows distinct structural properties as can be observed in the background images of Fig. 5. For artificial surfaces, the average roughness R_a can be scaled by scaling the width of the distribution of random numbers allowing us to determine h_{eff} for R_a up to 40 nm. As shown by the dotted line, the measured h_{eff} linearly depends on R_a with a constant of proportionality $c = 1.43$. The data obtained from the gold coated surface follows the same linear dependence demonstrating that the actual surface shape does not influence its effective position, but only the distribution of heights needs to be known.

The most important question to be answered by our simulations is the effect of a wrongly assumed position of a surface on experimental measurements. As mentioned in the introduction many groups use an approaching method to measure the slip length β. Here, a colloidal

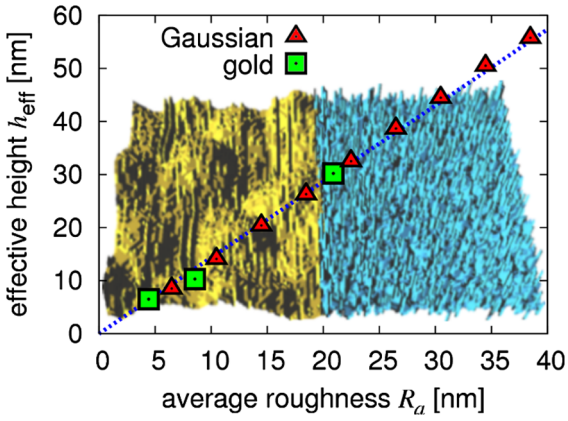

FIG. 5 (color online). (Color online) Simulated h_{eff} versus R_a for gold coated glass and a randomly generated surface with Gaussian distributed heights. The background image shows the gold surface (left) and the artificially generated structure (right).

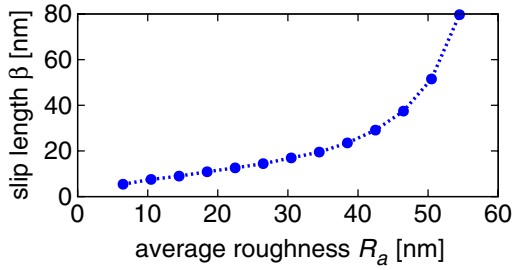

FIG. 6 (color online). (Color online) β versus R_a for water and randomly distributed roughness. By assuming $h_{\text{eff}} = h_{\text{max}}$, β is in the range of $h_{\text{max}} - h_{\text{eff}}$ for small R_a, but diverges for large R_a.

sphere at the tip of a cantilever immersed in a fluid is oscillated in the vicinity of a surface, or the cylinders of a surface force apparatus (SFA) are brought close to each other. The distance between the surfaces can become very small—even down to contact. To study the influence of the roughness on an apparent slip effect, we assume the surface to be placed at h_{max} as it is commonly done in experiments [13]. Then, we measure the slip length β by fitting Eq. (2). The wrong position of the surface causes a substantial error in the detected slip as can be inferred from Fig. 6. Here, β is given versus R_a for randomly generated boundaries with the heights of the surface obstacles following the Gaussian distribution given by the AFM data of the gold surface. For small R_a (and thus large separation of the plates) β is in the range of $h_{\text{max}} - h_{\text{eff}}$ and can be neglected in most practical cases. However, the detected slip diverges if R_a becomes large and grows to 80 nm for $R_a = 55$ nm. Here, a large R_a is equivalent to the channel width becoming very small—an effect also common in typical surface approaching experiments or microchannel flows. For curved surfaces, as they are utilized in SFA or AFM based slip measurements, the detected β can be even larger due to higher order components of the flow field. This might explain experiments reporting large slip lengths of $\beta \approx 100$ nm [3,20].

To conclude, we demonstrated that not properly taking into account surface structures of confining geometries can lead to substantial misinterpretations of measured flow properties. Especially since in typical setups not only roughness, but also, e.g., the wettability, electrostatic interactions or dissolved gasses influence the flow, it is essential for a correct understanding to separate the individual effects. We demonstrated that rough surfaces alone can lead to large apparent slip if the distance between boundaries is small—as it is typical in dynamic microfluidic experiments. These findings were obtained from LB simulations of flow between rough plates showing the existence of an imaginary effective plane where the no-slip boundary condition is valid. We compared our results to analytical calculations of Panzer *et al.* and found good agreement for small variations ($k < 1$). Large and more realistic perturbations ($k > 1$) can only be covered by simulations as presented here. By simulating flow of water along a gold coated surface and a randomly generated one with identical height distribution, we showed that the position of the effective plane is independent of the boundary structure and that only the height distribution is relevant. Further, these simulations depict the applicability of our method to real surface data. Simulations of flow along surfaces generated from AFM data allow to determine how detected slip might have to be corrected to take surface structures into account.

We thank H. Gong for the AFM data and O. I. Vinogradova, M. Rauscher, and M. Hecht for fruitful discussions. This work was financed within the DFG priority program "nano- and microfluidics" and by the "Landesstiftung Baden-Württemberg". Computations were performed at the Neumann Institute for Computing, Jülich.

[1] A. Stroock, S. Dertinger, G. Whitesides, and A. Ajdari, Anal. Chem. **74**, 5306 (2002).
[2] P. Joseph, C. Cottin-Bizonne, J. M. Benoi, C. Ybert, C. Journet, P. Tabeling, and L. Bocquet, Phys. Rev. Lett. **97**, 156104 (2006).
[3] C. Neto, D. Evans, E. Bonaccurso, H.-J. Butt, and V. Craig, Rep. Prog. Phys. **68**, 2859 (2005).
[4] C. Navier, Mem. Acad. Sci. Inst. Fr. **6**, 389 (1823).
[5] S. Richardson, J. Fluid Mech. **59**, 707 (1973).
[6] K. Jansons, Phys. Fluids **31**, 15 (1988).
[7] G. McHale and M. Newton, J. Appl. Phys. **95**, 373 (2004).
[8] A. Jabbarzadeh, J. D. Atkinson, and R. I. Tanner, Phys. Rev. E **61**, 690 (2000).
[9] B. Du, I. Doubaidoulline, and D. Johansmann, Langmuir **20**, 7794 (2004).
[10] M. Sbragaglia, R. Benzi, L. Biferale, S. Succi, and F. Toschi, Phys. Rev. Lett. **97**, 204503 (2006).
[11] F. Varnik, D. Dorner, and D. Raabe, J. Fluid Mech. **573**, 191 (2007).
[12] O. I. Vinogradova, Langmuir **11**, 2213 (1995).
[13] E. Bonaccurso, H.-J. Butt, and V. S. J. Craig, Phys. Rev. Lett. **90**, 144501 (2003).
[14] O. I. Vinogradova and G. E. Yakubov, Phys. Rev. E **73**, 045302(R) (2006).
[15] P. Panzer, M. Liu, and D. Einzel, Int. J. Mod. Phys. B **6**, 3251 (1992).
[16] S. Succi, *The Lattice Boltzmann Equation for Fluid Dynamics and Beyond* (Oxford Science Publications, Oxford, 2001).
[17] J. Harting, M. Harvey, J. Chin, M. Venturoli, and P. V. Coveney, Phil. Trans. R. Soc. A **363**, 1895 (2005).
[18] J. Harting, C. Kunert, and H. Herrmann, Europhys. Lett. **75**, 328 (2006).
[19] C. Kunert and J. Harting, Progress in CFD (to be published).
[20] E. Lauga, M. Brenner, and H. Stone, *Handbook of Experimental Fluid Dynamics* (Springer, New York, 2005), Chap. 15.